# Fabrication of Visible Light Active $MoS_2$–W–Cu Ternary Heterojunction for Enhanced Photocatalytic Degradation

R. Leelavathi[a], K. Vivekanandan[a,*] and V. Hariharan[b]

[a]*Department of Physics, Government Arts College, Coimbatore — 641018, Tamil Nadu, India*
[b]*Department of Physics, Mahendra Arts and Science College, Namakkal — 637 501, Tamil Nadu, India*

Received: 21.10.2023 & Accepted: 04.03.2024

Doi: 10.12693/APhysPolA.145.361 *e-mail: vivekgacprof@gmail.com

The increase in environmental pollution has led to a novel ternary photocatalytic system for remediation. These photocatalytic systems exhibit superior visible light active band gap of $Mo_{0.99}W_{0.005}Cu_{0.005}S_2$. A highly effective visible light active ternary heterojunction was fabricated using the hydrothermal method. Herein, it reports the hydrothermal synthesis of $MoS_2$–W–Cu as a photocatalyst, efficiently exhibiting greater photocatalytic activity for wastewater treatment under visible light. The photocatalytic degradation of methylene blue in aqueous suspension has been employed to evaluate the visible light photocatalytic activity of the prepared samples. The blue shift in the absorption onset confirms the size quantization of pure and doped $MoS_2$ nanoparticles, which act as effective and stable catalysts, making it possible to utilize visible light in photocatalysis. The as-prepared samples were characterized using field emission scanning electron microscope, energy dispersive X-ray analysis, X-ray diffraction, UV-visible, and UV-visible differential reflectance spectroscopy techniques. The characteristic Bragg peaks of $Mo_{0.99}W_{0.005}Cu_{0.005}S_2$ are reduced, indicating the possible formation of layered $MoS_2$. The field emission scanning electron microscope morphologies of $MoS_2$, $Mo_{0.99}W_{0.01}S_2$, and $Mo_{0.99}W_{0.005}Cu_{0.005}S_2$ are disordered, and nanorods were induced in the hydrothermal method. The calculated band gap of the novel photocatalyst was found from the differential reflectance spectroscopy plot, which helped in understanding the photo-induced electron–hole pair's recombination. $Mo_{0.99}W_{0.005}Cu_{0.005}S_2$ doping of ternary sample, which increases the photocatalytic degradation, was studied in detail and the experimental result is reported.

topics: $MoS_2$, ternary photocatalytic, hydrothermal, heterojunction

## 1. Introduction

The unprecedented increase in industry and cultivation may cause severe problems to the environment and economic life [1]. In the case of health and the environment, some serious risks are present, like an increase in pollutants, the use of large amounts of toxic dyes, and the presence of unsafe medicinal compounds in wastewater worldwide [2]. In day-to-day life, humans and the surrounding environment are exposed to tons of dangerous synthetic pollutants, which are constantly discharged from industries as well as from households and contain a certain compound that is very hard to decompose [3]. This kind of toxic material weakens the ecosystem and puts many species on the verge of extinction. In overcoming these problems, some methods can be helpful, like the microbial decomposition method, flocculation precipitation method, photocatalytic degradation method, etc. [4]. Among them, the most efficient and easiest way to remove these types of pollutants from wastewater is photocatalytic degradation since it is a technology with the potential to oxidize a great variety of complex organic compounds into simple molecules. It is equally important to find a suitable catalytic material, which needs to be beneficial to solve these problems and also needs to be environmentally friendly [5]. In the reformation of the environment and purification of water, semiconductor photocatalyst materials are used due to their good response [6]. Organic and inorganic pollutants are eliminated by using photocatalytic materials such as ZnO, $Fe_2O_3$, $TiO_2$, CdS, and $MoS_2$ [7]. Among these, $MoS_2$ has a better photoharvesting property and is a noble material, which is earth-abundant, metal-free, easy to synthesize, and has a morphological characteristic of delivering more active sites for pollutant observation [8]. Among the semiconductor materials, $MoS_2$ is the assuring material due to its efficiency in photocatalytic degradation and degradation under visible light in a promising way, enabling the development of a cost-effective and efficient photocatalyst material [4]. Many synthesis methods were developed to fabricate the $MoS_2$ nanostructures, such as hydrothermal method, chemical vapor deposition,

ball milling, laser pulsed deposition, electrochemical method, etc. Among these methods, the hydrothermal method has been preferred in the present study due to its low-temperature reaction, large production rate, and high purity of the obtained material [9–12].

$MoS_2$ is a two-dimensional material that attracts many researchers in industrial and scientific fields due to its possible application in sensors, photocatalysis, dye-sensitized solar cells, batteries, etc. [13]. It has a hexagonal crystalline structure of close-packed layered sulfur and molybdenum as a center layer, which makes it look like a sandwich structure, where Mo acts as an active catalyst site in $MoS_2$ [14]. In the application of photocatalysis, under the visible light region, the composites of molybdenum disulfide have maximum efficiency because of its properties such as optics, high chemical reactivity, and electrical carrier mobility, which is helpful in improving the absorption of light due to the charge carriers and has high mobility and increased surface area, thus making it a promising candidate for photocatalysis under the visible light [15].

Hasija et al. [8] reported an overview of enhancement in the photocatalytic oxidative ability of $MoS_2$ for water purification in their work, and they concluded that for better photo-oxidative property and charge carrier separation staggered type (II) $MoS_2$-based heterojunction is the better charge transfer method. Vattikuti et al. [16] provided a detailed overview of the photocatalytic performance of $MoS_2$ nanomaterials according to their structural components (single component, heterostructured) and highlighted the doped $MoS_2$ and their importance in the degradation of pollutants from contaminated wastewater through solar light irradiation. Mokari-Manshadiet al. [17] prepared mesoporous $MoS_2$ nanostructures using the facile hydrothermal approach for photodegradation of methylene blue compared with bulk, and it shows that within 15 min the mesoporous nanostructure removes 99.6% yields of methylene blue under visible light compared with bulk. Huang et al. [18] synthesized $MoS_2$ microspheres by the hydrothermal method using sodium molybdate and L-cysteine as the source materials and demonstrated the application of $MoS_2$ photocatalyst in thermal barrier coatings (TBC) degradation from environmental water samples (lake and river water), demonstrating its prospect in water treatment.

## 2. Experimental sections

### 2.1. Reagents

The synthesis of $MoS_2$ nanoparticles was carried out as $Mo_{1-x}W_xCu_yS_2$ ($x, y$=0) for pure, $Mo_{1-x}W_xS_2$ ($x$ = 0.01) for W-doped, $Mo_{1-x}W_xCu_yS_2$ ($x, y$=0.005) for Cu co-doped by ammonium heptamolybdatetetrahydrate ($(NH_4)_6Mo_7O_{24} \cdot 4H_2O$), thiourea ($CH_4N_2S$), sulphuric acid ($H_2SO_4$), sodium tungstate dihydrate ($Na_2WO_4 \cdot 2H_2O$), copper(II) sulfate pentahydrate ($CuSO_4 \cdot 5H_2O$), oleic acid, and double distilled water.

### 2.2. Experimental procedure

#### *2.2.1. Synthesis of pure $MoS_2$ (molybdenum disulphide)*

In order to synthesize pure $MoS_2$, certain parameters have to be maintained, such as the ratio of materials, solvent, optimized temperature, and timing of the reaction. The precursors, ammonium heptamolybdate tetrahydrate $(NH_4)_6Mo_7O_{24} \cdot 4H_2O$ and thiourea, were dissolved in 30 mL of distilled water and continuously stirred for thirty minutes at 80°C. The clear solution was then transferred to a 100 mL stainless steel autoclave and maintained at 80°C for 20 h and then allowed to cool down naturally to attain room temperature. The final product (black precipitate) was then washed thoroughly with water and ethanol to remove the impurities and kept in the oven for 8 h at 180°C for complete drying.

#### *2.2.2. Synthesis of W-doped $MoS_2$*

To synthesize tungsten (W)-doped $MoS_2$ nanoparticles, a similar inexpensive hydrothermal technique is used. Chemical precursors $(NH_4)_6Mo_7O_{24} \cdot 4H_2O$, thiourea, oleic acid, and $Na_2WO_4 \cdot 2H_2O$ were dissolved in 30 mL of distilled water and stirred for thirty minutes. The above solution was transferred into a 100 mL stainless steel autoclave and kept at 100°C for 20 h in an oven. The pressure inside the autoclave triggers the nucleation reaction. The sediments were collected and centrifuged with distilled water three to four times and then dried at 180°C for 8 h in the oven.

#### *2.2.3. Synthesis of W and Cu co-doped $MoS_2$*

Synthesis of tungsten and copper co-doped $MoS_2$ nanoparticles was carried out by changing many parameters to identify suitable conditions by a hydrothermal method. Precursors, $(NH_4)_6Mo_7O_{24} \cdot 4H_2O$, $Na_2WO_4 \cdot 2H_2O$, $CuSO_4 \cdot 5H_2O$, and thiourea, were dissolved in 30 mL of distilled water and stirred for 30 min. The suspension was transferred into a 100 mL stainless steel autoclave and kept at 100°C for 20 h. The final black product was centrifuged with ethanol and then allowed to dry for 8 h at 180°C in an oven.

### *2.2.4. Characterization*

The crystalline structure and phase purity of the samples were studied by X-ray diffraction (XRD), using Shimadzu XRD 6000 X-ray diffractometer Cu $K_\alpha$ radiation with $\lambda = 1.54$ Å in the $2\theta$ range of 5–80° at room temperature with a scanning rate of 0.06 deg/s. Fourier transform infrared (FTIR) spectra were recorded using a Brucker Tensor 27 spectrophotometer with a resolution of 2 $cm^{-1}$ in the range of 4000–400 $cm^{-1}$ at the regular KBr phase. The JEOL JSM field emission scanning electron microscope (FE-SEM) equipped with energy dispersive X-ray analysis (EDX) was used to find the surface morphology and elemental compositions presented in the prepared materials. Optical characterizations of the samples were performed using UV-visible spectroscopy (PerkinElmer UV/Vis/NIR spectrophotometer).

### *2.2.5. Photocatalytic activity test*

The corresponding photocatalytic activity of synthesized pure $MoS_2$, $Mo_{0.99}W_{0.01}S_2$, and $Mo_{0.99}W_{0.005}Cu_{0.005}S_2$ nanoparticles, prepared by the hydrothermal method, was investigated via the photodegradation of a chosen organic pollutant, i.e., methylene blue dye, under the illumination of visible light. The prepared samples containing around 50 mg of a catalyst material were dispersed in the ratio of 2:1 with methylene blue dye in an aqueous solution, such as a dye solution of (20 ml) within a quartz tube (40 ml). The respective suspension was stirred for 60 min in order to achieve adsorption equilibrium in the dark. Further, the obtained suspension was continuously irradiated under visible light. The process was continued every 15 min, and changes in the concentration of methylene blue in the suspension were monitored using a UV-Vis spectrophotometer (Ocean Optics, USA) in the range of 254 nm for short and 350 nm for long wavelengths. The maximum absorption of the chosen dye (methylene blue) was found to be 665 nm. The linear degradation nature of the proposed samples shows that the dye degrades in the visible infrared region (665 nm).

## 3. Results and discussion

XRD patterns of $MoS_2$, $Mo_{0.99}W_{0.01}S_2$, and $Mo_{0.99}W_{0.005}Cu_{0.005}S_2$ nanoparticles are shown in Fig. 1. XRD peaks indexed at $2\theta$ of 9°, 13°, 16°, 19°, 25°, 29°, and 38° correspond to the (120), (002), (100), (410), (221), (102), and (201) planes similar to the standard cards: (i) JCPDS card No. 37-1492, indicating that all diffraction peaks

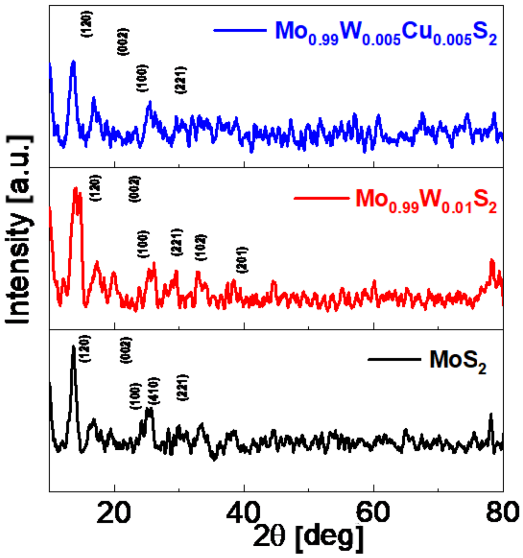


Fig. 1. XRD patterns of $MoS_2$, $Mo_{0.99}W_{0.01}S_2$, and $Mo_{0.99}W_{0.005}Cu_{0.005}S_2$ nanoparticles.

can readily confirm the hexagonal (2H–$MoS_2$) crystal structure [space group $P6_3/mmc$ (194)] with lattice constants $a = 2.91$ Å and $c = 12.03$ Å [19], and (ii) JCPDS card No. 87-2402, where the diffraction peaks are matched to the monoclinic ($WO_3$) crystal structure [space group $P_1c_1$] with lattice constants $a = 5.27$ Å, $b = 5.16$ Å, and $c = 7.67$ Å.

The high and sharp diffraction peak (002) belongs to as-prepared $MoS_2$, and doped samples indicate the formation of a well-stacked layered structure of $MoS_2$ during the hydrothermal process [15, 20, 21]. Some impurity peaks were observed during the analysis. The average crystallite size of $MoS_2$ nanoparticle was calculated by the X-ray line broadening method using Scherrer's equation, where $MoS_2$ has a crystalline size of 4.8 nm, whereas $Mo_{0.99}W_{0.01}S_2$ and $Mo_{0.99}W_{0.005}Cu_{0.005}S_2$ have a crystalline size of 6.7 nm and 4.8 nm, respectively. Some light shift is observed in the peaks due to the size of the tungsten ion being larger than in pure molybdenum ion.

The morphology of the prepared $MoS_2$, $Mo_{0.99}W_{0.01}S_2$, and $Mo_{0.99}W_{0.005}Cu_{0.005}S_2$ nanoparticles has been studied and confirmed using a field emission scanning electron microscope (FE-SEM). During hydrothermal synthesis, ammonium heptamolybdate and thiourea served as resources for molybdenum and sulfur. Therefore, the obtained $MoS_2$ samples demonstrate the attainment of optimized crystallinity. Moreover, in Fig. 2, it is clear that from pure $MoS_2$ the particles are too much larger, and they differ extensively in size and shape [22]. The surface morphology of the prepared $Mo_{0.99}W_{0.01}S_2$ sample exhibits richer defects due to the complete formation of ultra-thin nanosheets, which leads to the incorporation of tungsten in the sample [23]. In Fig. 2c, sample $Mo_{0.99}W_{0.01}S_2$ has a nanostructure in the richest form and has the

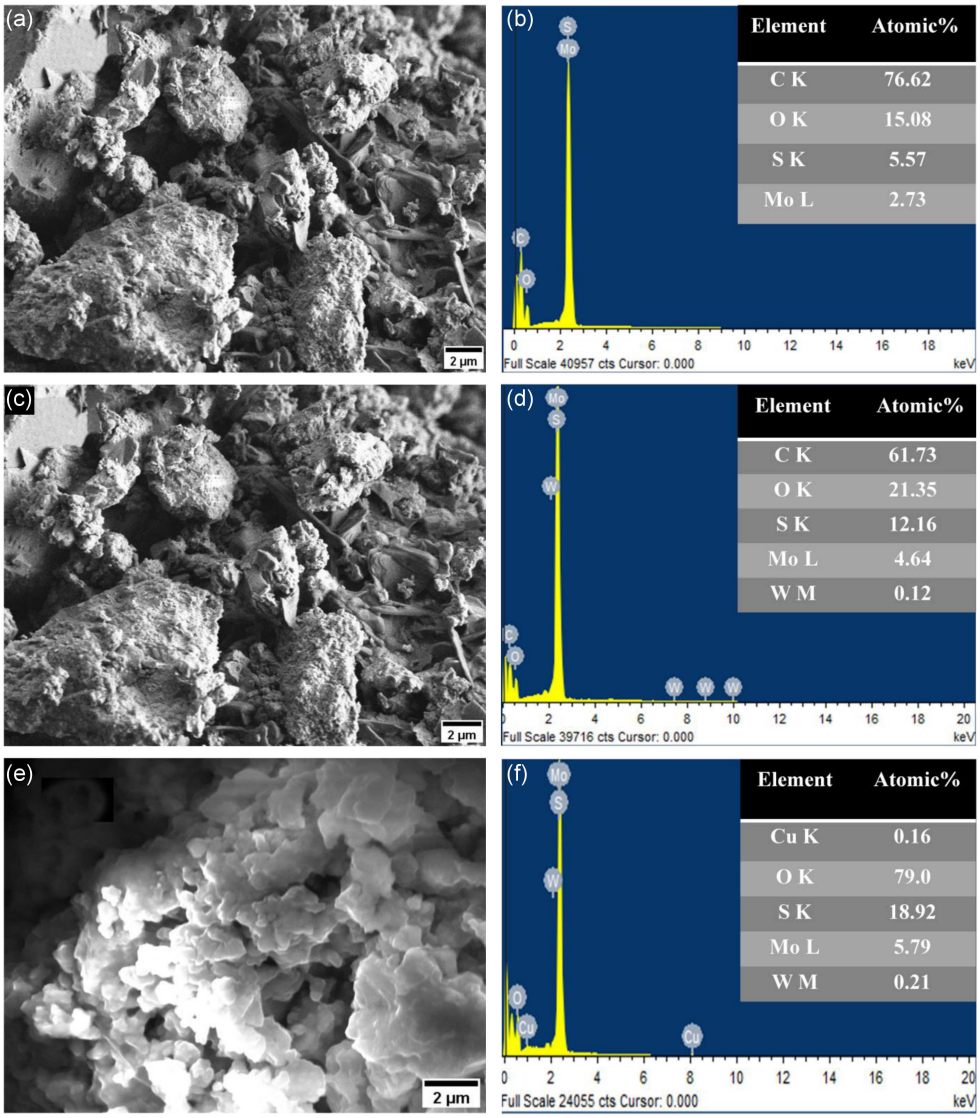


Fig. 2. (a) and (b) FE-SEM and EDAX pattern of $MoS_2$ nanoparticles, (c) and (d) FE-SEM and EDAX pattern of $Mo_{0.99}W_{0.01}S_2$, (e) and (f) FE-SEM and EDAX pattern $Mo_{0.99}W_{0.005}Cu_{0.005}S_2$ nanoparticles.

advantage that it covers a large surface area and is suitable for catalytic activity and photo harvesting property. The EDAX spectrum of the prepared $MoS_2$, $Mo_{0.99}W_{0.01}S_2$, and $Mo_{0.99}W_{0.005}Cu_{0.005}S_2$ nanoparticles show the composition and elemental distribution in the sample. Figure 2b shows the EDAX pattern of pure $MoS_2$, which confirms the presence of Mo and S, along with some impurities, such as O and C, obtained during the calcination process. Figure 2d shows the presence of the W dopant in the spectrum, along with some impurities during the hydrothermal reaction, where larger amounts of Mo atoms combine with S atoms to form $MoS_2S_2$.

Figure 3 shows the FTIR spectra of $MoS_2$, $Mo_{0.99}W_{0.01}S_2$, and $Mo_{0.99}W_{0.005}Cu_{0.005}S_2$. The band at 931.39 $cm^{-1}$ is due to the S–S bond [24]. The absorption band between 1100 and 1650 $cm^{-1}$ is due to the stretching vibrations of the hydroxyl group. The bands at around 1200 and 1650 $cm^{-1}$ are due to the presence of Mo–O vibrations [25]. The band at $\sim$ 600 $cm^{-1}$ is assigned to the Mo–S vibration [26]. S–S stretching is observed at 550 $cm^{-1}$, and other bands at 660, 1050, and 1400 $cm^{-1}$ can be assigned to sulphates [27].

Optical properties of $MoS_2$, $Mo_{0.99}W_{0.01}S_2$, and $Mo_{0.99}W_{0.005}Cu_{0.005}S_2$ nanoparticles were investigated by UV-Vis absorption spectroscopy. The shoulder peak is located at 306 nm, which is assigned to the blue shift [28]. The UV-Vis optical absorption spectra were recorded at room temperature in the wavelength range of 200–800 nm, as shown in Fig. 4a. In addition, the broad-band absorption centered at 270 nm (3.90 eV)–600 nm (2.75 eV) for $MoS_2$, 200 nm (3.90 eV)–350 nm (2.75 eV) for $Mo_{0.99}W_{0.01}S_2$, and 200 nm (3.90 eV)–550 nm (2.75 eV) for $Mo_{0.99}W_{0.005}Cu_{0.005}S_2$ result from transitions between regions with higher density of

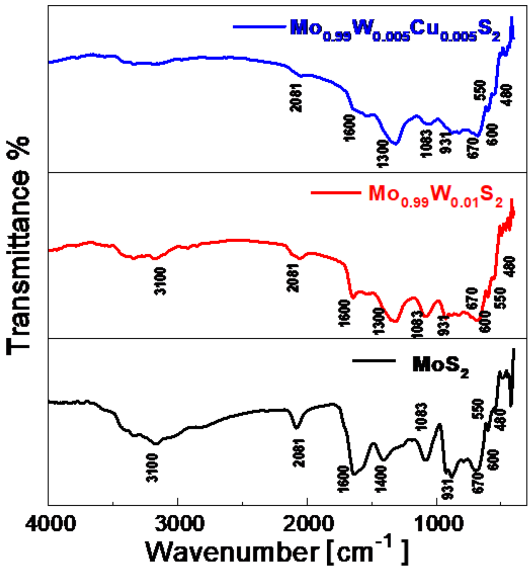


Fig. 3. FTIR spectrum of $MoS_2$, $Mo_{0.99}W_{0.01}S_2$, and $Mo_{0.99}W_{0.005}Cu_{0.005}S_2$ nanoparticles.

states [29]. The indirect band gap was calculated by the Tauc equation using the optical absorption data near the band edge, thus,

$$\sqrt{\alpha h\nu} = A\Big(h\nu - E_g\Big), \tag{1}$$

where $h\nu$ is the incident photon energy, and $A$ is a constant. Band gaps ($E_g$) are determined by linear extrapolation of the fit onto the $x$-axis [25, 30]. From the diffuse reflectance spectroscopy (DRS) plot, the calculated indirect band gap energies of the respected samples are 1.45 eV for $MoS_2$, 1.6 eV for $Mo_{0.99}W_{0.01}S_2$, and 1.68 eV for $Mo_{0.99}W_{0.005}Cu_{0.005}S_2$. In 1931, P. Kubelka and F. Munk presented a theory according to which the measured reflectance spectra can be transformed to the corresponding absorption spectra by applying the Kubelka–Munk function

$$F(R_\infty) = \frac{K}{S} = \frac{(1-R_\infty)^2}{2R_\infty}, \tag{2}$$

where $R_\infty = R_{\text{sample}}/R_{\text{standard}}$ is the reflectance of an infinitely thick specimen, while $K$ and $S$ are the absorption and scattering coefficients, respectively. Putting $R_\infty$ instead of $\alpha$ into (1) yields the form

$$\Big(F(R_\infty)h\nu\Big)^{1/\gamma} = B\big(h\nu - E_g\big). \tag{3}$$

The photocatalytic reaction is performed under the light radiation with an energy greater than or equal to the band gap energy ($E_g$). Then, there will be a movement of electrons from the valence band to the conduction band, thus leaving holes in the valence band behind. Electrons in the conduction band combine with $O_2$ to form superoxide radicals ($O^\bullet$). Subsequently, the holes in the valence band oxidize with water to form hydroxyl radicals ($OH^\bullet$). It leads to two possibilities: (i) due to the

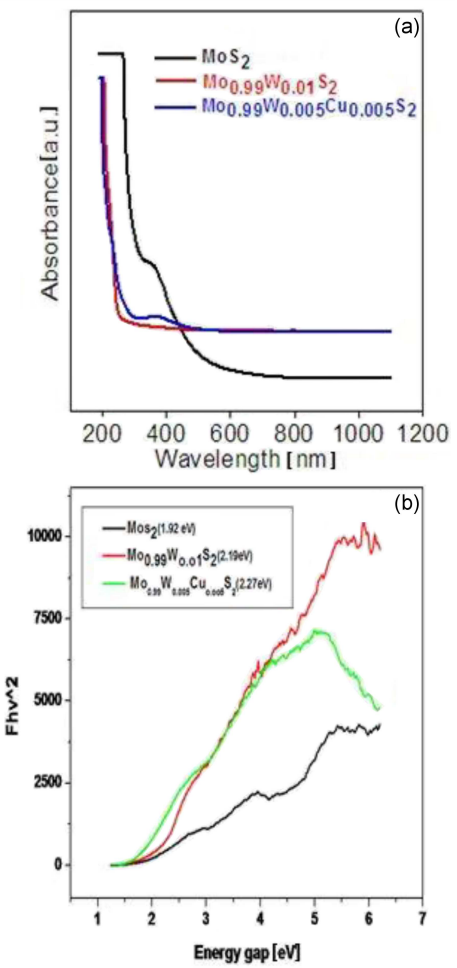


Fig. 4. (a), (b) UV-Vis spectrum of $MoS_2$, $Mo_{0.99}W_{0.01}S_2$, and $Mo_{0.99}W_{0.005}Cu_{0.005}S_2$.

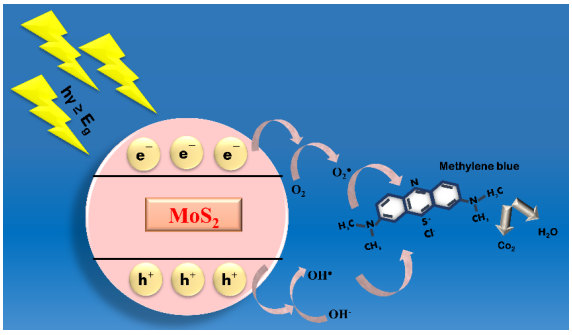


Fig. 5. Schematic representation of the degradation of methylene blue dye.

absence of suitable electron scavenging, there will be a recombination of the electron–hole ($e^-$–$h^+$) pair, which will produce thermal energy, and (ii) redox reaction takes place by avoiding recombination. Although the lifetime of an $e^-$–$h^+$ pair is a few nanoseconds, it is still long enough for promoting/initiating redox reactions. Thus, the series of chain oxidative–reductive reactions that occur

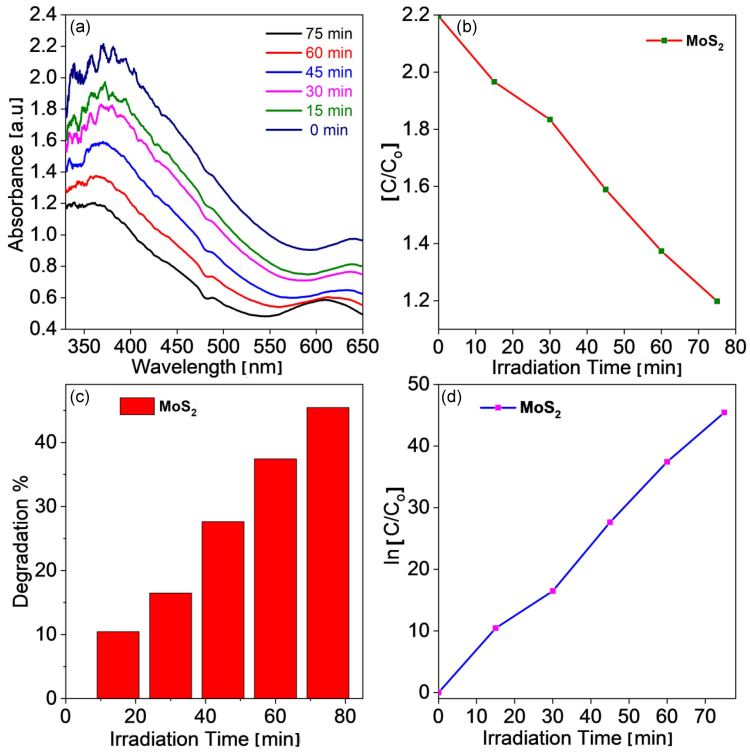


Fig. 6. (a) Photocatalytic activity of samples $MoS_2$ in MB dye degradation. (b) Kinetic curve for decomposition of MB over the prepared $MoS_2$ heterostructure in the presence of visible light under optimized reaction parameters. (c) Initial methylene blue (MB) concentration towards the degradation of MB under visible light using $MoS_2$.

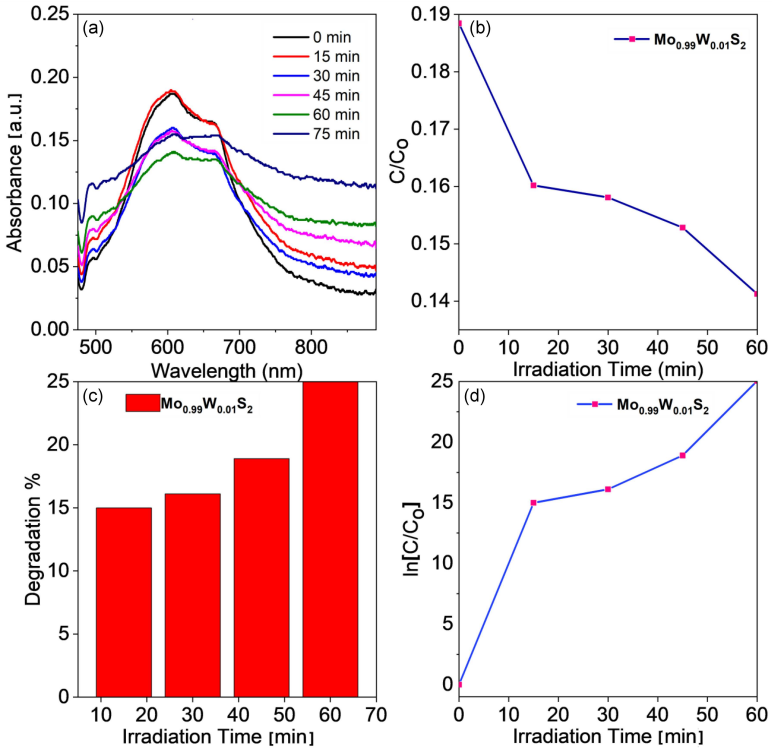


Fig. 7. a) Photocatalytic activity of samples $Mo_{0.99}W_{0.01}S_2$ in MB dye degradation. b) Kinetic curve for decomposition of MB over the prepared $Mo_{0.99}W_{0.01}S_2$ heterostructure in the presence of visible light under optimized reaction parameters. (c) Initial methylene blue (MB) concentration towards the degradation of MB under visible light using $MoS_2$.

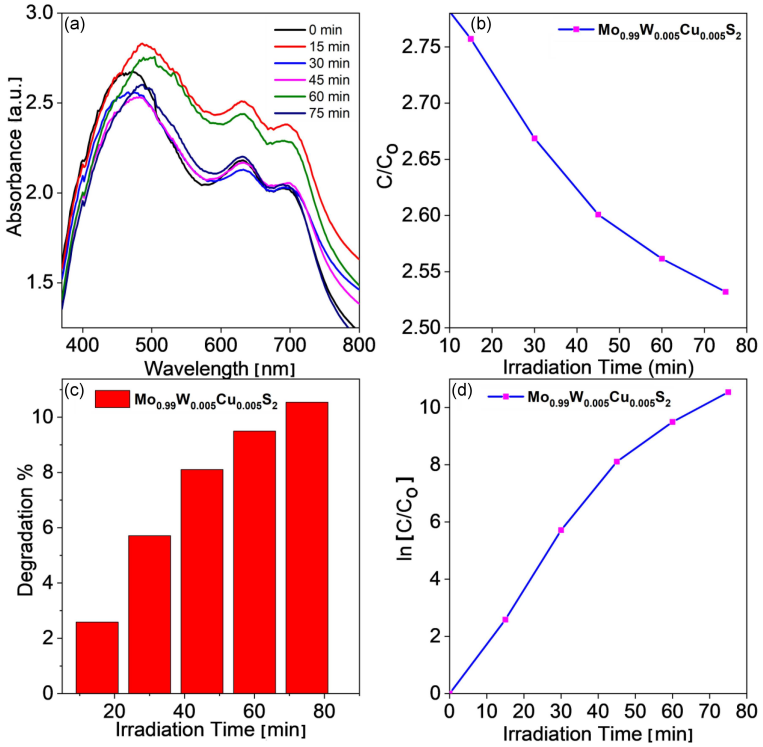


Fig. 8. (a) Photocatalytic activity of samples Mo0.99 $W_{0.005}Cu_{0.005}S_2$in MB dye degradation. (b) Kinetic curve for decomposition of MB over the prepared $Mo_{0.99}W_{0.005}Cu_{0.005}S_2$ heterostructure in the presence of visible light under optimized reaction parameters. (c) Initial methylene blue (MB) concentration towards the degradation of MB under visible light using Mo0.99 $W_{0.005}Cu_{0.005}S_2$.

at the photon-activated surface lead to the degradation of organic molecules present in the pollutant [31, 32].

To calculate the absorption of methylene blue (MB) dye, the measurement of its removal efficiency of $MoS_2$ and doped mixtures were used at different time intervals. From the initial values, its percentage derivatives were calculated to determine the removal of pollutants using $MoS_2$ and doped mixtures [17]. Figure 5 shows the schematic representation of the degradation of methylene blue dye.

The reactions were performed at 15 min intervals under visible light, and the absorption peak of MB dye appears at 370 nm for $MoS_2$, 605 nm for $Mo_{0.99}W_{0.01}S_2$, and 485 nm for $Mo_{0.99}W_{0.005}Cu_{0.005}S_2$. At the time of reaction, the absorbance shows no difference, but the dye concentration is proportional to its absorption [2].

Degradation efficiency was determined by employing the equation

$$\text{degradation} = \frac{C_0 - C}{C_0} \times 100\%, \tag{4}$$

where $C_0$ is the MB concentration at the initial state, and $C$ is the MB concentration after illuminating under visible light at a specified time [33]. Using the MB dye as an organic pollutant, photocatalytic materials prove their efficiency through a cationic dye, which has an organic compound of clear absorbance property in the visible light region, which is helpful in removing the organic pollutants from the water resources, thus making the whole approach one of the most efficient methods [34].

The kinetics of a degradation process of methylene blue was determined using a pseudo-first-order kinetic model equation

$$\ln\left(\frac{C_0}{C}\right) = k\,t, \tag{5}$$

where $C_0$ and $C$ are the concentrations of MB before and after exposure to natural sunlight, respectively, $k$ is the reaction rate constant acquired from the slope of the graph, and $t$ is their radiation time for the reaction.

Using $MoS_2$, $Mo_{0.99}W_{0.01}S_2$, and $Mo_{0.99}W_{0.005}Cu_{0.005}S_2$ as a photocatalyst material, the MB dye was successfully removed by around 45% to 83%, as seen in Figs. 6–8. In 75 min, the degradation was increased up to 83% by adding the suitable dopant material to the source material. Using tungsten as a dopant material, the removal was enhanced from 45% to 62%, as seen in Fig. 7. At the same time, $Mo_{0.99}W_{0.005}Cu_{0.005}S_2$-doped material shows a similar increase in degradation efficiency, i.e., from 62% to 83% in Fig. 8. The oxidation of MB is detected from the peak values based on the relationship between $\ln(C_0/C)$ and $t$. From the pseudo-first-order kinetics equation,

the estimated rate constant value for $MoS_2$, $Mo_{0.99}W_{0.01}S_2$, and $Mo_{0.99}W_{0.005}Cu_{0.005}S_2$ samples were found to be 0.0409 $min^{-1}$, 0.1577 $cm^{-1}$, and 0.0393 $cm^{-1}$, respectively.

The total percentage of methylene blue dye removal was calculated for $MoS_2$ (45%), $Mo_{0.99}W_{0.01}S_2$ (62%), and $Mo_{0.99}W_{0.005}Cu_{0.005}S_2$ (83%). According to the plotted diagrams, it was observed that the amount of photocatalytic degradation for $Mo_{0.99}W_{0.005}Cu_{0.005}S_2$ nanomaterials has increased by 83% compared to pure $MoS_2$ and $Mo_{0.99}W_{0.01}S_2$. The results of the methylene blue dye degradation under visible light irradiation over the prepared samples are given in Figs. 6–8. It can be found that $Mo_{0.99}W_{0.005}Cu_{0.005}S_2$ nanomaterials show higher photocatalytic activity.

## 4. Conclusions

Pure and doped $Mo_{0.99}W_{0.01}S_2$ and $Mo_{0.99}W_{0.005}Cu_{0.005}S_2$ nanoparticles were successfully prepared using a hydrothermal method. The effect of temperature and suitable dopants on the morphology transformation has been reported. The XRD results indicate that the diffraction can be readily observed as hexagonal 2H–$MoS_2$ and monoclinic $WO_3$ with lattice constants $a = 5.27$ Å, $b = 5.16$ Å, and $c = 7.67$ Å. From the UV-Vis spectra, the optical absorption data and optical band gap energies were estimated, and there is a change in the band gap of $MoS_2$ due to the addition of W and Cu, which helps in its application. The FTIR spectra show the fundamental vibrations of the $MoS_2$ material and its doped samples. The photocatalytic behavior of the $Mo_{0.99}W_{0.005}Cu_{0.005}S_2$ nanoparticles increased from 45% to 83% due to the suitable dopant added to the source material. In the case of tungsten as a doping material, the efficiency was enhanced from 45% to 62%, and at the same time, the doped $Mo_{0.99}W_{0.005}Cu_{0.005}S_2$ material shows the increasing efficiency in degradation, i.e., from 62% to 83%.

## References


[1] M. Ge, C. Cao, J. Huang, S. Li, Z. Chen, K.Q. Zhang, S.S. Al-Deyab, Y. Lai, *J. Mater. Chem. A* **4**, 6801 (2016).

[2] S.E. Islam, D.-R. Hang, C.-H. Chen, K.H. Sharma, *Chem. Eur. J.* **24**, 9305 (2018).

[3] K. He, G. Chen, G. Zeng, A. Chen, Z. Huang, J. Shi, T. Huang, M. Peng, L. Hu, *Appl. Catal. B Environ.* **228**, 19 (2018).

[4] F. Yang, Z. Zhang, Y. Wang, M. Xu, W. Zhao, J. Yan, C. Chen, *Mater. Res. Bull.* **87**, 119 (2017).

[5] J. Theerthagiri, R.A. Senthil, B. Senthilkumar, A.R. Poluc, J. Madhavan, M. Ashokkumar, *J. Solid State Chem.* **252**, 43 (2017).

[6] J. Singh, Rishikesh, S. Kumar, R.K. Soni, *J. Alloys Compd.* **849**, 156502 (2020).

[7] M.I. Khan, M.S. Hasan, K.A. Bhatti, H. Rizvi, A. Wahab, Shafique-ur Rehman, M.J. Afzal, A. Nazneen, M.F. Khan, A. Nazir, M. Iqbal, *Mater. Res. Express.* **7**, 015061 (2020).

[8] V. Hasija, P. Raizada, V.K. Thakur, A.A.P. Khan, A.M. Asiri, P. Singh, *J. Environ. Chem. Eng.* **8**, 104307 (2020).

[9] U. Krishnan, M. Kaur, G. Kaur, K. Singh, A.R. Dogra, M. Kumar, A. Kumar, *Mater. Res. Bull.* **111**, 212 (2019).

[10] J. Pu, Y. Yomogida, K.-K. Liu, L.-J. Li, Y. Iwasa, T. Takenobu, *Nano Lett.* **12**, 4013 (2012).

[11] W. Zhang, P. Zhang, Z. Su, G. Wei, *Nanoscale* **7**, 18364 (2015).

[12] A. Ramadoss, T. Kim, G.-S. Kim, S.J. Kim, *New J. Chem.* **38**, 2379 (2014).

[13] Y. Li, F. Xiang, W. Lou, X. Zhang, *IOP Conf. Ser. Earth Environ. Sci.* **300**, 052021 (2019).

[14] H. Adhikari, C. Ranaweera, R. Gupta, S.R. Mishra, *MRS Adv.* **1**, 3089 (2016).

[15] A. Rani, K. Singh, A.S. Patel, A. Chakraborti, S. Kumar, K. Ghosh, P. Sharma, *Chem. Phys. Lett.* **738**, 136874 (2020).

[16] S.V.P. Vattikuti, C. Byon, in: *Nanoscaled Films and Layers*, Ed. L. Nanai, IntechOpen, London 2017, p. 239.

[17] M.H. Mokari-Manshadi, M. Mahani, Z. Hassani, D. Afzali, E. Esmaeilzadeh, *J. Nanosci. Nanotechnol.* **17**, 8864 (2017).

[18] S. Huang, C. Chen, H. Tsai, J. Shaya, C. Lu, *Sep. Purif. Technol.* **197**, 147 (2018).

[19] K. Shomalian, M.M. Bagheri-Mohagheghi, M. Ardyanian, *J. Mater. Sci. Mater. Electron.* **28**, 14331 (2017).

[20] S.X. Hou, *Ceramics-Silikaty* **61**, 158 (2017).

[21] Y. Wang, X. Li, C. Wang, *J. Non-Oxide Glasses* **9**, 47 (2017).

[22] B. Pourabbas, B. Jamshidi, *Chem. Eng. Sci.* **138**, 55 (2008).

[23] J.N. He, Y.Q. Liang, J. Mao, X.M. Zhang, X.J. Yang, Z.D. Cui, S.L. Zhu, Z.Y. Li, B.B. Li, *J. Electrochem. Soc.* **163**, H299 (2016).

[24] K.C. Lalithambika, K. Shanmugapriya, S. Sriram, *Appl. Phys. A* **125**, 817 (2019).

[25] S.V.P. Vattikuti, C. Byon, Ch.V. Reddy, J. Shim, B. Venkatesh, *Appl. Phys. A* **119**, 813 (2015).

[26] K.-J. Huang, J.-Z. Zhang, G.-W. Shi, Y.M. Liu, *Electrochim. Acta* **132**, 397 (2014).

[27] H. Akram, C. Mateos-Pedrero, E. Gallegos-Suárez, N. Allali, T. Chafik, I. Rodriguez-Ramos, A.G. Ruiz, *J. Nanosci. Nanotechnol.* **12**, 6679 (2012).

[28] W. Gu, Y. Yan, C. Zhang, C. Ding, Y. Xian, *ACS Appl. Mater. Interfaces* **8**, 11272 (2016).

[29] X. Man, L. Yu, J. Sun, S. Li, *Funct. Mater. Lett.* **9**, 1650065 (2016).

[30] S.V.P. Vattikuti, C. Byon, Ch.V. Reddy, B. Venkatesh, J. Shim, *J. Mater. Sci.* **50**, 5024 (2015).

[31] M.N. Chong, B. Jin, C.W.K. Chow, C. Saint, *Water Res.* **44**, 2997 (2010).

[32] J. Bussi, M. Ohanian, M. Vázquez, E.A. Dalchiele, *J. Environ. Eng.* **128**, 733 (2002).

[33] Ritika, M. Kaur, A. Umar, S.K. Mehta, S. Singh, S.K. Kansal, H. Fouad, O.Y. Alothman, *Materials* **11**, 2254 (2018).

[34] S.A. Darsara, M. Seifi, M.B. Askari, *Optik (Stuttg.)* **169**, 249 (2018).